ACS APPLIED MATERIALS & INTERFACES

Research Article

www.acsami.org

Evaluation of Heterocycle-Modified Pentathiophene-Based Molecular Donor Materials for Solar Cells

Qing-Cai Yu,[†,‡] Wei-Fei Fu,[§,‡] Jun-Hua Wan,[*,†,⊥] Xiao-Feng Wu,[†] Min-Min Shi,[*,§] and Hong-Zheng Chen[§]

[†]Key Laboratory of Organosilicon Chemistry and Material Technology of Ministry of Education, Hangzhou Normal University, Hangzhou 310012, People's Republic of China

[§]State Key Laboratory of Silicon Materials, MOE Key Laboratory of Macromolecular Synthesis and Functionalization, and Department of Polymer Science and Engineering, Zhejiang University, Hangzhou 310027, People's Republic of China

[⊥]State Key Laboratory of Molecular Engineering of Polymers, Fudan University, Shanghai 200433, People's Republic of China

Supporting Information

ABSTRACT: Two novel solution-processable acceptor−donor−acceptor (A−D−A)-structured organic small molecules with diketopyrrolopyrrole (**DPP**) as terminal acceptor units and pentathiophene (**PTA**) or pyrrole-modified pentathiophene (**NPTA**) as the central donor unit, namely, **DPP$_2$(PTA)** and **DPP$_2$(NPTA)**, were designed and synthesized. We examined the effects of changing the central bridging heteroatoms of the five-ring-fused thienoacene core identity from sulfur [**DPP$_2$(PTA)**] to nitrogen [**DPP$_2$(NPTA)**] in the small-molecule donor material. Replacement of the bridging atom with a different electronic structure has a visible effect on both the optical and electrical properties: **DPP$_2$(NPTA)**, which contains much more electron-rich pyrrole in the central thienoacene unit, possesses red-shifted absorption and a higher HOMO level relative to **DPP$_2$(PTA)** with the less electron-rich thiophene in the same position. More importantly, substitution of the bridging atoms results in a change of the substituting alkyl chains due to the nature of the heteroatoms, which significantly tailored the crystallization behavior and the ability to form an interpenetrating network in thin-film blends with an electron acceptor. Compared to **DPP$_2$(PTA)** with no alkyl chain substituting on the central sulfur atom of the **PTA** unit, **DPP$_2$(NPTA)** exhibits improved crystallinity and better miscibility with $PC_{71}BM$ probably because of a dodecyl chain on the central nitrogen atom of the **NPTA** unit. These features endow the **DPP$_2$(NPTA)**/$PC_{71}BM$ blend film higher hole mobility and better donor/acceptor interpenetrating network morphology. Optimized photovoltaic device fabrication based on **DPP$_2$(NPTA)**/$PC_{71}BM$ (1.5:1, w/w) has resulted in an average power conversion efficiency (PCE) as high as 3.69% (the maximum PCE was 3.83%). This study demonstrates that subtle changes and tailoring of the molecular structure, such as simply changing the bridging heteroatom in the thienoacene unit in D/A-type small molecules, can strongly affect the physical properties that govern their photovoltaic performances.

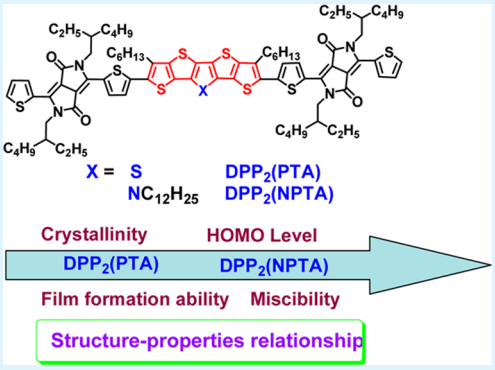

KEYWORDS: *solution-processable small molecule, organic solar cell, cycle extension, heterocycle-modified pentathiophene, diketopyrrolopyrrole, structure−property relationship*

INTRODUCTION

Solution-processed narrow-band-gap small molecules, used as the donor component in bulk-heterojunction (BHJ) organic solar cells (OSCs), have received more attention recently owing to their unique advantage of good batch-to-batch reproducibility of the photovoltaic performance, which benefits from their high purity and definite molecular structure.[1−6] Thus far, a high power conversion efficiency (PCE) of >7% has been reported from several solution-processed small molecules,[7−11] approaching that of polymer solar cells. Nevertheless, their overall performance is still significantly behind that of their polymer counterparts. Generally, a high-efficiency small-molecule donor should meet several key requirements, such as a broad and strong absorption, suitable lowest unoccupied molecular orbital (LUMO) and highest occupied molecular orbital (HOMO) levels, high hole mobility, excellent film formation ability, and miscibility with fullerene derivatives.[3] Currently, the most useful method to enhance the PCE is to optimize both orbital energy levels and morphological behaviors via molecular design on solution-processed small-molecule donor materials.. In addition, compared to polymers, the relatively short conjugated backbone of small molecules increases the tendency to crystallize but reduces the capacity to form interpenetrating network morphology with fullerene

Received: January 28, 2014
Accepted: April 1, 2014
Published: April 1, 2014

   dx.doi.org/10.1021/am5006223 | ACS Appl. Mater. Interfaces 2014, 6, 5798−5809

derivatives.[12,13] Therefore, an understanding of the fundamental structure−property−function relationships of small-molecule donors is needed for the design of materials with improved PCE.

Specifically, the introduction of the planar heteroarenes into π-conjugated polymers[14−16] and organic small-molecule[17−20] backbones as donor units has been proven to be able to bring several desirable characteristics into the relative materials, such as higher charge mobility and broader light absorption owing to increasing effective conjugation length by facilitating π-electron delocalization, ideal for a number of organic electronic applications including solar cells and field-effect transistors. Interestingly, He et al. had found that, upon increasing the number for fused thiophene rings as donor units from three to five, the packing structures of the relative polymers were obviously improved.[21] Most recently, Peng et al.'s studies have demonstrated that replacing benzodithiophene (**BDT**) with a naphthodithiophene (**NDT**) building block in a diketopyrrolopyrrole (**DPP**)-based copolymer resulted in enhanced absorption, higher hole mobility, and low-lying HOMO energy levels, which are beneficial for improving the photovoltaic parameters in OSCs.[22] Similar results were reported by Marks and co-workers, who had also studied how the sizes and shapes of thienoacenes affect the hole mobility and photovoltaic performances in **DPP**-based small molecules.[23−25] Obviously, cyclic extension on the donor unit has been expected to enhance the charge mobility and adjust the energy levels besides extending conjugation. In addition, further tuning of the electron-donating ability and other physical properties of these thienoacenes can be achieved by changing the bridged heteroatoms of the donor units.[14]

Typical planar donor units are heteroatom-bridged bithiophenes, a three-ring-fused system, such as cyclopenta[2,1-*b*:3,4-*b*′]dithiophene (**CPT**),[26−28] dithieno-[3,2-*b*:2′,3′-*d*]silole (**DTS**),[29−31] dithieno[3,2-*b*:2′,3′-*d*]pyrrole (**DTP**),[32−35] and dithieno[3,2-*b*:2′,3′-*d*]thiophene (**DTT**).[36−40] Inspired by the benefits of a bigger thienoacene, such as band-gap reduction and charge-mobility enhancement,[41−44] we thus direct our attention toward cycle extension of heteroatom-bridged bithiophenes and their incorporation as donor units into D/A-type small molecules for OSC application.

The π-extended **DTT** derivatives (pentathiophene, **PTA**) were reported several years ago and exhibited noticeably high hole mobility.[45] However, to the best of our knowledge, the **PTA** unit has not been introduced into low-band-gap conjugated materials (both polymer and small molecules) for solar cell application so far. It is noteworthy that the pyrrole-modified pentathiophene (**NPTA**) has not been synthesized as yet.

As such, to shed light on the cycle extension of heteroatom-bridged bithiophene, herein we separately utilized these thienoacenes as central donor units and the widely reported building block of **DPP**[46−52] as the acceptor unit, thereby obtaining two symmetric A−D−A-structured molecules, as shown in Scheme 1. According to the different thienoacenes in the central position of the two synthesized molecules, they were named **DPP$_2$(PTA)** and **DPP$_2$(NPTA)**, respectively.

Furthermore, in this contribution, we demonstrated that the central heteroatoms (sulfur vs nitrogen) within the donor unit of small molecules could not only effectively modulate the electronic structure but also pronouncedly impact the self-assembly and crystalline behaviors by introducing different types of alkyl chains, such as no alkyl chain substituting on the sulfur atom but one alkyl chain substituting on the nitrogen atom. Meanwhile, we found that the alkyl chain substituting on the central heteroatom of the **NPTA** unit also played an important role in the film formation ability and miscibility with $PC_{71}BM$.

Scheme 1. Structure of Small Molecules

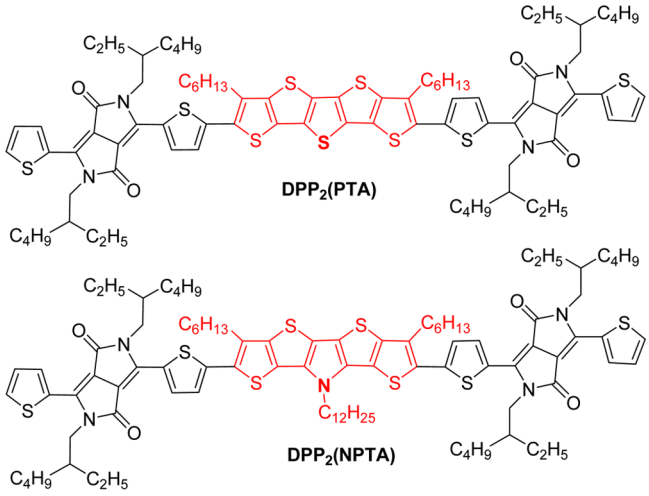

Although the effect of the heteroatoms in specific positions on the electronic properties has been widely investigated, the relationship between the morphological structure and the heteroatom in the D/A-type small-molecule system has not been extensively studied so far.[53] Because the well-defined small-molecule system allows us to better correlate variations in the molecular structure with relevant properties, it is anticipated that the structure−property relationships revealed in this study provided a useful reference for the improved design and understanding of D/A-type narrow-band-gap π-conjugated small molecules and polymers to maximize efficiency in the pursuit of more promising candidates.

RESULT AND DISCUSSION

Synthesis and Characterization. Generally, the synthesis of the two novel D/A-type molecules involves four procedures, i.e., cycle extension of heteroatom-bridged bithiophene units, then introduction of functional groups to these thienoacenes, synthesis of the monobromo-substituted diketopyrrolopyrrole (**4**), and a coupling reaction. Considering the limited solubility of five linearly fused ring units, two hexyl chains were designedly attached on the β positions of two terminal thiophene rings in **PTA** and **NPTA**. Scheme 2 shows the synthetic route to cycle extension of heteroatom-bridged bithiophene units. **PTA** was synthesized by treating compound **1** with *n*-BuLi at −78 °C to produce the corresponding dianion, which was then quenched with commercial bis(phenylsulfonyl) sulfide, whereas **NPTA** was attained by palladium-catalyzed Buchwald−Hartwig coupling of compound **1** and dodecylamine (see Scheme 2).

In order to synthesize the target D/A-type molecules via the more environmentally friendly Suzuki coupling reaction, the two thienoacenes were then transformed into the corresponding diboronic ester derivatives. Both **2** and **3** were successfully prepared directly from **PTA** and **NPTA** by a typical deprotonation−isopropyl pinacol borate quenching procedure. Finally, the two designed D/A small molecules, **DPP$_2$(PTA)** and **DPP$_2$(NPTA)**, were achieved with acceptable yield

dx.doi.org/10.1021/am5006223 | ACS Appl. Mater. Interfaces 2014, 6, 5798−5809

Scheme 2. Synthesis of the Two Small Molecules

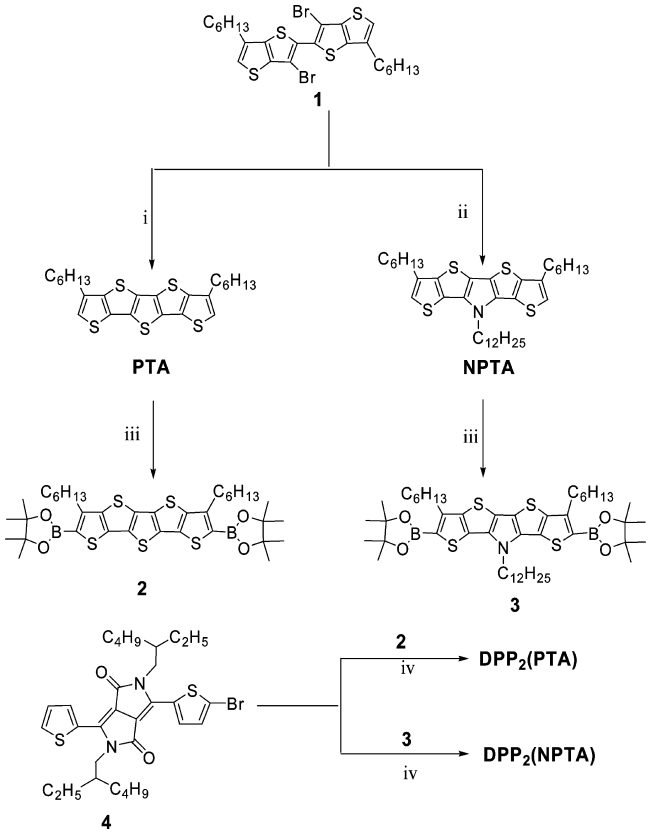

(i) *n*-BuLi/THF, −78 °C, $(PhSO_2)_2S$, 33%; (ii) Pd_2dba_3, NaO*t*-Bu, BINAP, *n*-dodecylamine/toluene, 40%; (iii) *n*-BuLi/THF, −78 °C to room temperature, isopropoxyboronic acid pinacol ester, 35% for compound **2** and 40% for compound **3**; (iv) $Pd(PPh_3)_4$, K_2CO_3, Aliquat 336, toluene/H_2O, 85 °C, 24 h, 40% for **DPP$_2$(PTA)** and 25% for **DPP$_2$(NPTA)**.

through Suzuki cross-coupling of compound **4** with diboronic ester compounds **2** and **3**, respectively.

The target small molecules were fully characterized by ^1H and ^{13}C NMR, matrix-assisted laser desorption ionization time-of-flight mass spectrometry (MALDI-TOF-MS), and high-resolution mass spectrometry (HRMS; see the Experimental Section). Both small molecules are readily soluble in common organic solvents, including CH_2Cl_2, $CHCl_3$, tetrahydrofuran (THF), toluene, chlorobenzene, and dichlorobenzene at room temperature.

Thermal Properties. Thermogravimetric analysis (TGA) and differential scanning calorimetry (DSC) in a nitrogen atmosphere were performed to investigate the thermal properties of the two small molecules, as outlined in Figure 1. TGA analysis reveals that 5% weight-loss temperatures (T_d) of **DPP$_2$(PTA)** and **DPP$_2$(NPTA)** are 338 and 392 °C, respectively (Figure 1a), indicating that the two small molecules are thermally stable enough for their application in solar cells. As shown in Figure 1b, the main melting endotherm occurs at 250 °C for **DPP$_2$(PTA)** and 247.3 °C for **DPP$_2$(NPTA)** because of the existence of long alkyl chain substituting on the nitrogen atom of the **NPTA** unit. Upon cooling, both **DPP$_2$(PTA)** and **DPP$_2$(NPTA)** exhibit a major crystallization exotherm at 209.8 and 214.9 °C, respectively, manifesting that the two molecules have an obvious tendency to crystallize. Noticeably, on the basis of a comparison of the associated enthalpy values ΔH (kJ mol^{-1}) for the phase transition, one can find that the degree of crystallinity for **DPP$_2$(NPTA)** is obviously higher than that for **DPP$_2$(PTA)**. In addition, this can also be confirmed by the much narrower both endothermic and exothermic peaks of **DPP$_2$(NPTA)** relative to those of **DPP$_2$(PTA)**.

Morphology and Microstructure. The crystalline behaviors of **DPP$_2$(PTA)** and **DPP$_2$(NPTA)** were further evaluated using optical microscopy (OM) equipped with a temperature controller. Surprisingly, crystallization occurred when the melted **DPP$_2$(PTA)** and **DPP$_2$(NPTA)** cooled slowly. **DPP$_2$(PTA)** showed one-dimensional (1D) micrometer wires with a diameter from hundreds of nanometers to several micrometers and a length of about hundreds of micrometers (Figure 2a), while **DPP$_2$(NPTA)** formed a two-dimensional (2D) sisal-like structure with a sharp tip (Figure 2b). It is well-known that the assembly morphologies of materials are controlled by their intermolecular interactions. Such different morphologies indicated the significant change of intermolecular interactions in the two materials. It is reasonable to consider that the dodecyl chain substituting on the nitrogen atom in the **NPTA** unit contributes to the variation of intermolecular interactions in **DPP$_2$(NPTA)** compared to **DPP$_2$(PTA)**.[54,55]

Wide-angle X-ray scattering (WAXS) is a powerful technique to characterize the molecular order of semiconducting polymers and small molecules. Here, we use WAXS to determine differences in the molecular arrangement of the two small

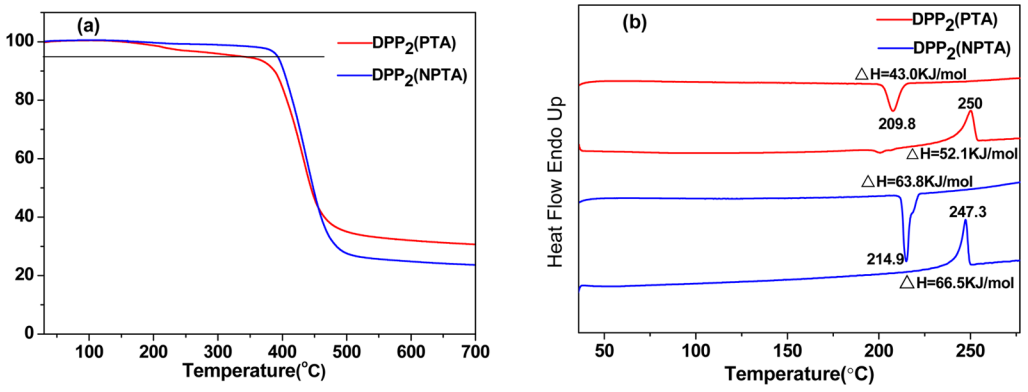

Figure 1. (a) TGA curves with a heating rate of 10 °C min^{-1} under a nitrogen atmosphere and (b) DSC thermograms at 10 °C min^{-1} in the temperature range from 30 to 300 °C for **DPP$_2$(PTA)** and **DPP$_2$(NPTA)**.

dx.doi.org/10.1021/am5006223 | ACS Appl. Mater. Interfaces 2014, 6, 5798−5809

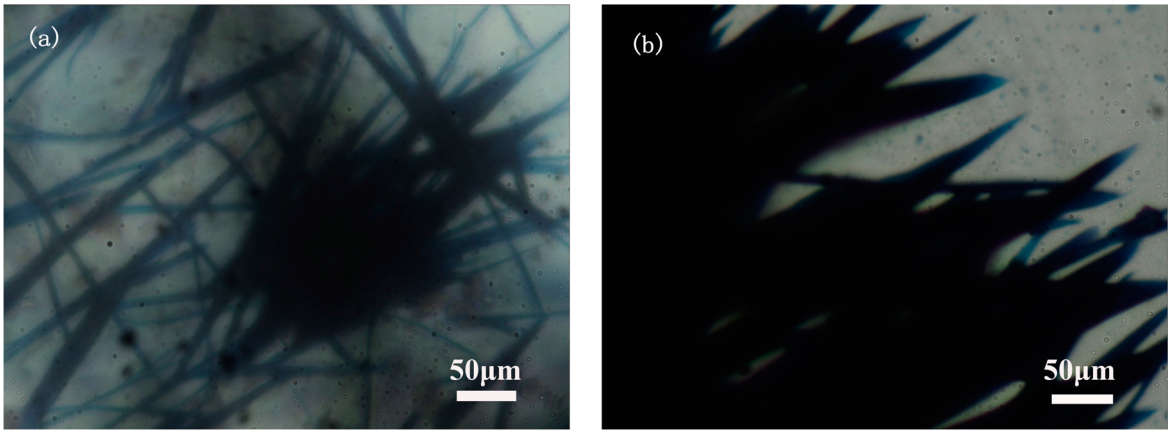

Figure 2. OM images of samples obtained by slow cooling of the completely melted (a) **DPP$_2$(PTA)** and (b) **DPP$_2$(NPTA)**.

molecules in powders. From Figure 3, powders of **DPP$_2$(PTA)** and **DPP$_2$(NPTA)** exhibit strong reflections with q at 3.59 and

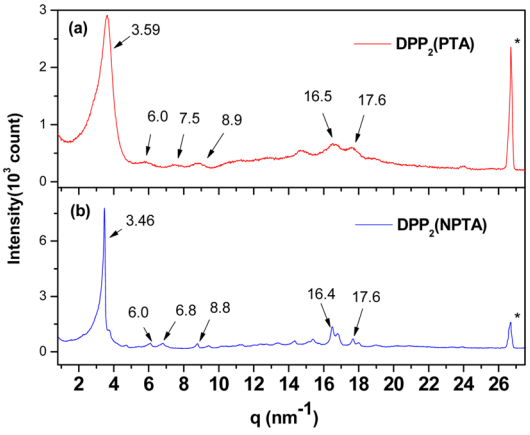

Figure 3. WAXS of **DPP$_2$(NPTA)** and **DPP$_2$(PTA)** powdered samples in aluminum foil. The scattering vector is defined as $q = 4\pi \sin(\theta)/\lambda$, where λ is the incident X-ray wavelength and θ is half of the scattering angle. The 1D plot represents the azimuthally integrated intensity from the 2D detector. Asterisks indicate the reflection of aluminum foil.

3.46 nm^{-1}, respectively, corresponding to d spacings between the molecular layers of 1.74 and 1.82 nm. Generally, the reflection at this area is attributed to stacking along the long alkyl side chains.[53,56] Compared to **DPP$_2$(PTA)**, a bigger d spacing is observed for **DPP$_2$(NPTA)**, which is in accordance with its longer alkyl (dodecyl) chain. Interestingly, as for **DPP$_2$(NPTA)**, the reflections (6.0, 6.8, and 8.8 nm^{-1}) of the peaks are found and combined with the first reflection (3.46 nm^{-1}) following a ratio of $1:3^{1/2}:4^{1/2}:7^{1/2}$, which can be assigned to (100), (110), (200), and (001) reflections from a hexagonal columnar structure. The intense reflections at q between 16.4 and 17.6 nm^{-1} are attributed to $\pi-\pi$ stacking distances (3.5−3.8 Å). As shown in Figure 3b, besides the reflection (100) with q at 3.59 nm^{-1}, (110), (200), and (001) reflections are also found for **DPP$_2$(PTA)**, which indicates the presence of crystalline domains with the same packing structures as those of **DPP$_2$(NPTA)**, while the relatively broad and weak reflections [(110), (200), and (001)] suggest a lower degree of crystalline content in **DPP$_2$(PTA)** relative to **DPP$_2$(NPTA)**. It is worth noting that the appearance of a broad hump centered at q = 16 nm^{-1} reveals that a certain number of amorphous domains are embodied in the crystalline powder for **DPP$_2$(PTA)**.[57] This point is consistent with the result obtained from the DSC experiment.

This result provides additional evidence that the alkyl chains substituting on the central heteroatom of the thienoacene unit play an important role in modulating the self-assembly behavior of small molecules. It is understandable that the rigid and planar skeleton of the **PTA** unit provides **DPP$_2$(PTA)** a degree of crystalline property, while besides the same planar skeleton, an additional alkyl chain substituting on the nitrogen atom in the **NPTA** unit in all probability helps to self-assemble **DPP$_2$(NPTA)** into more ordered supramolecular structure.[58,59]

Optical Properties. The absorption spectra of **DPP$_2$(PTA)** and **DPP$_2$(NPTA)** in dilute CH_2Cl_2 solutions and in thin films are shown in Figure 4. The corresponding optoelectronic data

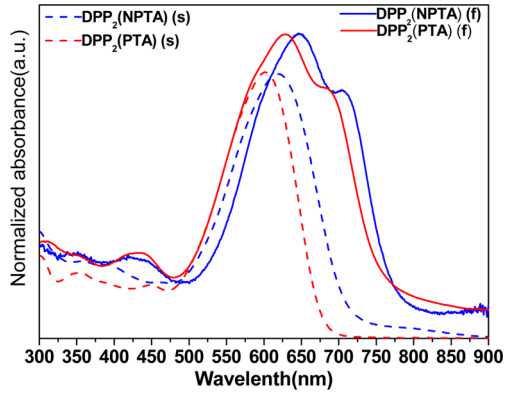

Figure 4. UV/vis absorption spectra of **DPP$_2$(NPTA)** and **DPP$_2$(PTA)** in CH_2Cl_2 solutions and in solid films on the quartz plate. The absorption spectra for solution was normalized (dashed lines); the absorption spectra for films was normalized and multiplied by 1.2 (solid lines).

are summarized in Table 1. In CH_2Cl_2 solution, both small molecules show only one main absorption band with maxima at 600 and 620 nm, respectively, which originates from intermolecular charge transfer (ICT) between the donor and acceptor units. Obviously, the donor units have a remarkable influence on the absorptions owing to the adjustments in the electronic structure of thienoacenes accomplished by the central heterocycles, such as thiophene as the center structural unit of **PTA** and pyrrole as the the center structural unit of **NPTA**, respectively. As we know, pyrrole is much more

dx.doi.org/10.1021/am5006223 | ACS Appl. Mater. Interfaces 2014, 6, 5798−5809

Table 1. Summary of the Absorption, Optical Band Gap, and HOMO Level of Small Molecules

compound	λ_{max}^{sol} (nm)	E_g^{opt} (eV)[a]	λ_{max}^{film} (nm)	E_g^{opt} (eV)[b]	HOMO (eV)[c]	LUMO (eV)[c]	HOMO (eV)[d]	LUMO (eV)[d]
DPP_2(PTA)	600	1.82	629	1.59	−5.10	−3.58	−4.81	−2.77
DPP_2(NPTA)	620	1.73	648	1.55	−4.96	−3.67	−4.70	−2.70

[a]Optical band gap was derived from the absorption onset of solutions. [b]Optical band gap was derived from the absorption onset of films. [c]HOMO and LUMO energy levels were calculated in terms of the oxidation and reduction onset potentials according to the equation HOMO/LUMO = −(4.50 + E_{onset}) eV. [d]HOMO and LUMO energy levels were calculated with the *Gaussian 03* program with DFT-B3LYP-6-31G*.

electron-rich than thiophene. So, the **NPTA** unit should have much stronger electron-donating ability than the **PTA** unit. This leads to a more pronounced ICT between the **NPTA** and acceptor units; therefore, the absorption peak of **DPP_2(NPTA)** is remarkably red-shifted compared to that of **DPP_2(PTA)**.

On going from solution to film, the absorption bands of **DPP_2(PTA)** and **DPP_2(NPTA)** in films are significantly broadened, extending the absorption onset to 782 and 795 nm, respectively, and both of them show a new vibronic peak at the long-wavelength direction close to the absorption edge, indicating that some well-ordered structure exists in the solid state.[48,60−62] Moreover, the vibronic structure of the absorption for **DPP_2(NPTA)** is much more pronounced, which demonstrated that molecule stacking may be much stronger in the film of **DPP_2(NPTA)** relative to **DPP_2(NPTA)**. Apparently, this is also consistent with the results gained from investigation of the crystallinity and morphology. The optical band gaps of films are 1.59 eV for **DPP_2(PTA)** and 1.55 eV for **DPP_2(NPTA)**.

Electrochemical Properties. The redox properties of the two molecular materials were determined by cyclic voltammetry in CH_2Cl_2 solutions of 0.1 M tetrabutylammonium hexafluorophosphate ($TBAPF_6$) using a platinum wire as the counter electrode and a saturated calomel electrode (SCE) as the reference electrode. Figure 5 shows the cyclic voltammograms of the two small molecules in CH_2Cl_2, and the data are summarized in Table 1. As shown in Figure 5, both of the two small molecules undergo a reversible multiple-electron oxidation originating from successive oxidation of the thienoacene unit and two **DPP** units. Similarly, a reversible reduction process is observed in both small molecules. The onset potential of a ferrocene/ferrocenium (Fc/Fc^+) redox couple is found to be 0.30 V relative to the SCE reference electrode in our measurement system, and the energy level of Fc/Fc^+ was assumed to be at −4.8 eV under vacuum.[63] Thus, the HOMO and LUMO energy levels of compounds in solution can be estimated from the onset potentials for oxidation and reduction from the equation of $E_{HOMO/LUMO}$ = −exp($E_{(ox/re)}$ + 4.50) (eV). The onset oxidation potentials (E_{ox}) are 0.60 V versus SCE for **DPP_2(PTA)** and 0.46 V versus SCE for **DPP_2(NPTA)**, which correspond to the HOMO energy levels of −5.10 and −4.96 eV, respectively. As expected, the heteroatoms in the central position of the thienoacene unit can effectively modulate the HOMO levels of D/A-type molecules. Owing to the pyrrole, **NPTA** has a much stronger electron-donating ability than **PTA**, thereby endowing **DPP_2(NPTA)** with a much higher oxidation potential and HOMO level. In the same way, the LUMO energy levels were obtained as −3.58 eV for **DPP_2(PTA)** and −3.67 eV for **DPP_2(NPTA)**.

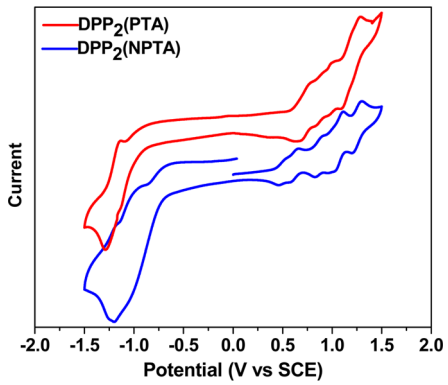

Figure 5. Cyclic voltammograms of small molecules in CH_2Cl_2 solution with the SCE reference electrode. Scan rate: 100 mV s^{-1}.

Besides, density functional theory (DFT) was also used to predict the HOMO and LUMO energy levels of the new small molecules at the B3LYP/6-31G* level. The calculated HOMO and LUMO levels of **DPP_2(PTA)** were −4.81 and −2.77 eV, respectively, while the corresponding levels for **DPP_2(NPTA)** were predicted to be −4.70 and −2.70 eV, respectively (see the Supporting Information). Although the DFT-predicted energy levels are overestimated, the trend of the HOMO for the two molecules is in good accordance with those determined by electrochemical measurements.

Considering that $PC_{61}BM$ or $PC_{71}BM$ has HOMO and LUMO energy levels of around −5.90 and −3.91 eV,[64] respectively, when the two novel D/A-type molecules are used as donor materials and $PC_{61}BM$ or $PC_{71}BM$ as the acceptor material for the fabrication of OSCs, a large enough driving force for excition dissociation and charge generation can be expected.

Photovoltaic Performance. To investigate the potential of the two D/A-type molecules as electron donors in an OSC, BHJ OSCs were fabricated with a conventional device structure of indium−tin oxide (ITO)/poly(3,4-ethylenedioxythiophene):poly(styrenesulfonate) (PEDOT:PSS)/photoactive layer/poly[(9,9-bis(3′-(*N*,*N*-dimethylamino)propyl)-2,7-fluorene)-*alt*-2,7-(9,9-dioctylfluorene)] (PFN)/Al and tested under simulated 100 mW cm^{-2} AM 1.5G illumination. The photoactive layer is a blend of small molecules and $PC_{71}BM$ in varied blend ratios and spin-coated from $CHCl_3$ solutions. First, we performed the optimization of photovoltaic performance of the OSCs by changing the D/A weight ratios. Table 2 reveals that the different optimized D/A weight ratios were observed for the OSC-based **DPP_2(PTA)** and **DPP_2(NPTA)**, 1:1 with a PCE of 2.09% for the former and 1:2 with a PCE of 2.00% for the latter. In addition, it should be mentioned that the devices based on **DPP_2(PTA)** show higher PCEs than those based on **DPP_2(NPTA)** in the case of D/A ratios at 2:1, 1:1, and 1:2. The relatively higher short-circuit current density (J_{sc}) and fill factor (FF) for the former suggest an improved phase separation in corresponding active layers (vide infra).

Generally, thermal annealing of the film before and after evaporation of the metal cathode significantly increases the device performance of BHJ solar cells owing to the improve-

Table 2. Summary of the Photovoltaic Performance of Solution-Processed OSCs Based on Small Molecules/$PC_{71}BM$ Blends in $CHCl_3$

compound	D/A ratio	DIO (v/v %)	annealing temp (°C)	V_{oc} (V)[a]	J_{sc} (mA cm^{-2})[a]	FF (%)[a]	PCE (%)[a]
DPP_2(PTA)	2:1			0.78 (±0.01)	3.07 (±0.12)	32.2 (±1.0)	0.77 (±0.06)
	1:1			0.78 (±0.01)	5.95 (±0.25)	45.3 (±1.6)	2.09 (±0.10)
	1:2			0.76 (±0.01)	5.81 (±0.27)	47.0 (±1.0)	2.06 (±0.10)
	1:1		100	0.77 (±0.01)	6.82 (±0.50))	45.7 (±2.0)	2.39 (±0.10)
	1:1	0.25	100	0.75 (±0.01)	6.12 (±0.58)	45.7 (±1.0)	2.09 (±0.16)
DPP_2(NPTA)	2:1			0.76 (±0.01)	1.50 (±0.06)	27.1 (±0.8)	0.30 (±0.01)
	1.5:1			0.76 (±0.01)	2.17 (±0.02)	28.0 (±0.4)	0.45 (±0.01)
	1:1			0.76 (±0.01)	4.95 (±0.21)	32.6 (±1.1)	1.23 (±0.03)
	1:2			0.76 (±0.01)	7.20 (±0.14)	36.5 (±1.2)	2.00 (±0.02)
	2:1		100	0.73 (±0.01)	9.13 (±0.17)	44.9 (±1.4)	2.98 (±0.09)
	1.5:1		100	0.72 (±0.01)	10.27 (±0.34)	45.0 (±1.1)	3.33 (±0.02)
	1:1		100	0.76 (±0.01)	8.90 (±0.12)	44.4 (±1.2)	2.89 (±0.15)
	1:2		100	0.76 (±0.01)	5.43 (±0.06)	33.7 (±1.1)	1.39 (±0.06)
	1.5:1	0.25	100	0.71 (±0.01)	10.69 (±0.28)	48.3 (±1.0)	3.69 (±0.12)
	1.5:1	0.40	100	0.69 (±0.01)	7.02 (±0.80)	51.2 (±2.0)	2.49 (±0.25)

[a]Average value from eight devices.

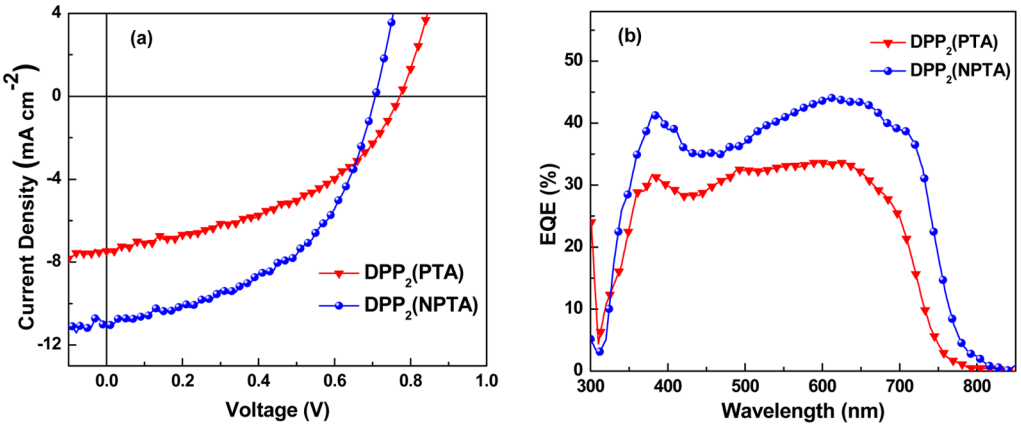

Figure 6. (a) $J-V$ characteristics and (b) EQE of the optimized BHJ solar cells prepared from different small molecules/$PC_{71}BM$.

ment in the morphology of the active layer. Encouragingly, an obvious enhancement in the PCEs upon thermal annealing has been attained for both **DPP_2(PTA)**- and **DPP_2(NPTA)**-based devices, especially for the latter. Indeed, for the optimized device based on the **DPP_2(PTA)**:$PC_{71}BM$ layer (1:1, w/w), an enhancement in J_{sc} from 5.95 to 6.82 Am cm^{-2} with the open-circuit voltage (V_{oc}) and FF remaining relatively constant, results in a moderate improvement of PCE (2.39%) after thermal annealing at 100 °C for 10 min. However, a deterioration of the performance is observed in the initial optimized device based on the **DPP_2(NPTA)**:$PC_{71}BM$ layer (1:2, w/w) upon thermal annealing at 100 °C. Interestingly, thermal annealing led to significant improvement in both J_{sc} and FF and, in turn, facilitated the device based on the **DPP_2(NPTA)**:$PC_{71}BM$ layer (1.5:1, w/w) delivery of a significant photovoltaic performance with PCE up to 3.33% at 100 °C. The PCE could be further improved to 3.69% (the maximum PCE was 3.83%) after the use of 0.25% 1,8-diiodooctane (DIO) as an additive to optimize the morphology of the active layer. Probably, in this system, DIO helps to form efficient percolation channels for charge transport,[65] which results in higher J_{sc} and FF despite slightly decreased V_{oc}. The current density–voltage ($J-V$) characteristics of the optimized devices are presented in Figure 6a.

As we expected, the optimized devices based on the two small molecules exhibited different V_{oc}, which is directly related to the energy difference between the HOMO of the donor and the LUMO of the acceptor. The optimized device based on **DPP_2(NPTA)** shows a lower V_{oc} of 0.71 V than that of **DPP_2(PTA)** (0.77 V). This is in accordance with the fact that the HOMO level of **DPP_2(NPTA)** is higher than that of **DPP_2(PTA)**. Also, it is interesting to find that the optimized device based on **DPP_2(NPTA)** presents both higher J_{sc} (10.69 mA cm^{-2}) and FF (48.3%) than that based on **DPP_2(PTA)** (6.82 mA cm^{-2} and 45.7%), which reveals a more effective charge transport in OSCs based on **DPP_2(NPTA)**. This can be verified by the charge mobility and film morphology (vide infra). Additionally, the lower optical band gap of **DPP_2(NPTA)** also contributes to the higher J_{sc}.

In order to show the photon-to-electron conversion efficiencies of the devices at different wavelengths, corresponding external quantum efficiencies (EQEs) of the devices were measured under illumination of a monochromatic light source. The EQE curves of the optimized OSCs based on small molecules/$PC_{71}BM$ are shown in Figure 6b. The EQE curve for the optimized device based on **DPP_2(PTA)** exhibits an effective photoconversion efficiency from 300 to 700 nm with a EQE value at around 24%. By comparison, the EQE value of the device based on **DPP_2(NPTA)** reaches 34%, and it shows a

dx.doi.org/10.1021/am5006223 | ACS Appl. Mater. Interfaces 2014, 6, 5798–5809

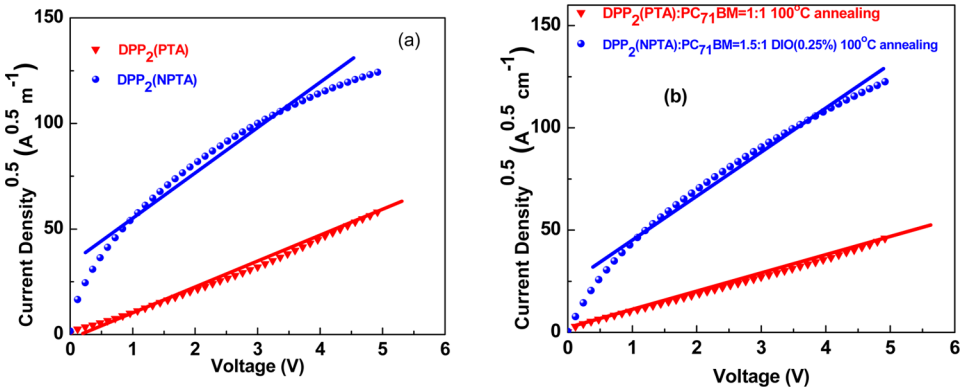

Figure 7. $J^{0.5}-V$ curves of hole-only devices for (a) ITO/PEDOT:PSS/small molecule/MoO_3/Al and (b) ITO/PEDOT:PSS/small molecules/$PC_{71}BM$/MoO_3/Al. The symbols represent experimental data, and the solid lines are fitted according to the Mott−Gurney law.

remarkably broader EQE response (300 to 800 nm) than the device based on **DPP$_2$(PTA)**, which results in a higher J_{sc}. These results also confirm that replacing the central sulfur atom of **PTA** with a nitrogen atom could significantly improve the photoconversion efficiency and broaden the response range.

Charge-Carrier Mobility. The hole mobilities of pristine films for small molecules were measured by the space-charge-limited-current (SCLC) method, and the $J-V$ curves are shown in Figure 7a. The films of both of two small molecules exhibit hole mobilities on the order of 10^{-4} cm^2 V^{-1} s^{-1}, with 0.50×10^{-4} cm^2 V^{-1} s^{-1} for **DPP$_2$(PTA)** and 1.62×10^{-4} cm^2 V^{-1} s^{-1} for **DPP$_2$(NPTA)**. Apparently, the hole mobility of **DPP$_2$(NPTA)** is 3 times higher than that of **DPP$_2$(PTA)**. This fact is consistent with the results from DSC and WAXS investigations, which showed improved crystallinity in the solid sample of **DPP$_2$(NPTA)**.

Considering that the photovoltaic performance is closely related to the charge-transport properties of the active layer, we further investigated the hole mobilities of the active layers (Figure 7b). It has been found that the hole mobilities decreased evidently when mixed with $PC_{71}BM$. The average hole mobility for a **DPP$_2$(NPTA)**/$PC_{71}BM$ (1.5:1, w/w) blend film cast from $CHCl_3$ (0.25% DIO) upon annealing at 100 °C is 1.33×10^{-4} cm^2 V^{-1} s^{-1}, which is 6 times higher than that (0.20×10^{-4} cm^2 V^{-1} s^{-1}) of a **DPP$_2$(PTA)**/$PC_{71}BM$ (1:1, w/w) film upon annealing at 100 °C. The obviously high hole mobility of the **DPP$_2$(NPTA)**/$PC_{71}BM$ film accounts for higher J_{sc} and better FF of the corresponding device.

Morphologies of the Active Layers. The morphology of the photoactive layer is very important for the photovoltaic performance of OSCs. The surface morphologies of the blend films of small molecules/$PC_{71}BM$ spin-coated from a chloroform solution were studied by tapping-mode atomic force microscopy (AFM). Figure 8 displays the AFM height and phase images of small molecules/$PC_{71}BM$ blend films showing the best photovoltaic performance. From Figure 8a,c, it can be seen that uneven and anomalistic shape features with varying average diameters from 100 to 200 nm were observed for a **DPP$_2$(PTA)**/$PC_{71}BM$ (1:1, w/w) film cast from $CHCl_3$ upon annealing at 100 °C. The low film formation ability and miscibility may be due to their intrinsic aggregation, resulting from the high rigidity and planarity of the molecular backbone as well as the low miscibility with fullerene derivatives due to the lack of enough side chains in **DPP$_2$(PTA)**. A similar result had been also observed in the blend-film-based **DTTDPP** with analogous structure, which consists of **DTT** as the central

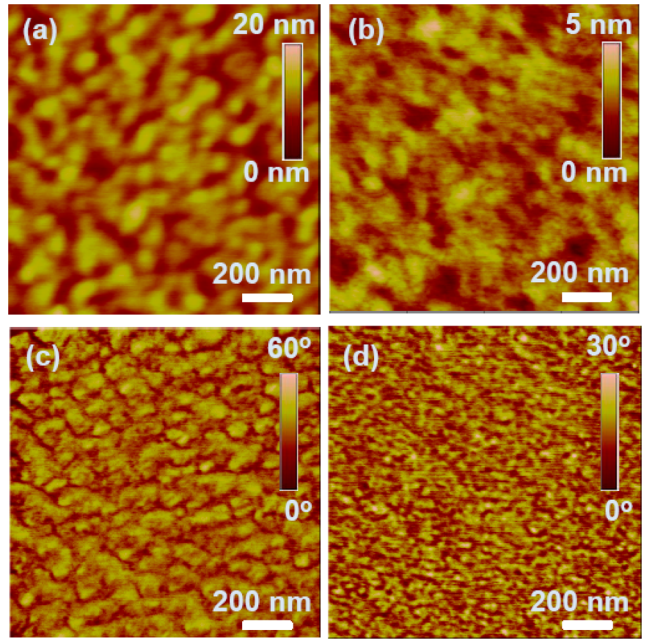

Figure 8. AFM height images (a and b) and phase images (c and d) of the optimized blend films: (a and c) **DPP$_2$(PTA)**:$PC_{71}BM$ = 1:1 upon 100 °C annealing; (b and d) **DPP$_2$(NPTA)**:$PC_{71}BM$ = 1.5:1 DIO(0.25%) upon 100 °C annealing.

donor unit and two **DPP** as terminal acceptor units.[36] Such large aggregated domains could decrease the exciton dissociation efficiency because the exciton diffusion length for most organic semiconductors is estimated to be in the range of 5−20 nm.[66,67] Interestingly, the phase images in Figure 8b,d demonstrate that the donor/acceptor interpenetrating network of a **DPP$_2$(NPTA)**/$PC_{71}BM$ (1.5:1, w/w) blend film cast from $CHCl_3$ (0.25% DIO) upon annealing at 100 °C is better than that of **DPP$_2$(PTA)**/$PC_{71}BM$ (1:1, w/w), and the desired phase separation is achieved. This nanostructured texture in a **DPP$_2$(NPTA)**/$PC_{71}BM$ (1.5:1, w/w) blend film provides better percolation pathways for the generated charge carriers, which is consistent with higher hole mobility and efficiency.

For comparison, the morphologies of small molecules/$PC_{71}BM$ (1:1, w/w) without annealing and without DIO additive were also investigated (Figure 9). As shown in Figure 9a,b, the root-mean-square roughness is 1.60 nm for **DPP$_2$(PTA)**/$PC_{71}BM$ (1:1, w/w) and 0.44 nm for **DPP$_2$(NPTA)**/$PC_{71}BM$ (1:1, w/w), respectively, indicating

dx.doi.org/10.1021/am5006223 | ACS Appl. Mater. Interfaces 2014, 6, 5798−5809

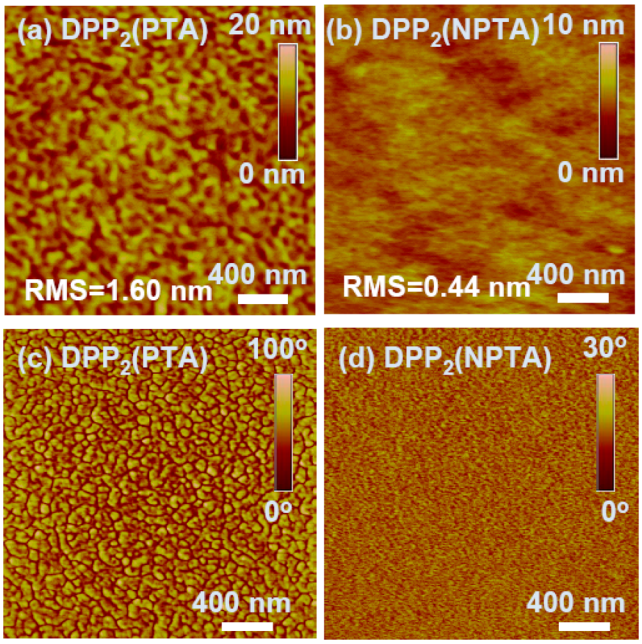

Figure 9. AFM height images (a and b) and phase images (c and d) of small molecule/$PC_{71}BM$ blend films: (a and c) **DPP_2(PTA)**:$PC_{71}BM$ = 1:1; (b and d) **DPP_2(NPTA)**:$PC_{71}BM$ = 1:1.

better miscibility between **DPP_2(NPTA)**and $PC_{71}BM$. Phase images of the two films show different features, as shown in Figure 9c,d. The **DPP_2(PTA)**/$PC_{71}BM$ (1:1, w/w) film shows a continuous phase separation, with the domain sizes ranging from 50 to 100 nm, whereas no obvious nanoscale phase separation is observed in a **DPP_2(NPTA)**/$PC_{71}BM$ (1:1, w/w) film. Thus, the device based on **DPP_2(PTA)**/$PC_{71}BM$ (1:1, w/w) shows better J_{sc}, FF and PCE than the device based on **DPP_2(NPTA)**/$PC_{71}BM$ (1:1, w/w).

According to a comparison of the morphologies of the active layers before and after thermal annealing or the addition of DIO (Figures 8 and 9), one can find that a **DPP_2(NPTA)**/$PC_{71}BM$ blend film is more sensitive to thermal annealing and DIO additive. It is obvious that thermal annealing and the addition of DIO as a cosolvent help self-organization of the active layer and produce nanoscale phase separation.

On the basis of the AFM investigation, the two small molecules exhibited different miscibility and phase separation with the $PC_{71}BM$. **DPP_2(PTA)**, with no alkyl chain substituting on the central heteroatom, has a lower miscibility with $PC_{71}BM$ and larger self-aggregated domains, while long dodecyl chain substituting on the nitrogen atom in the **NPTA** unit probably endows **DPP_2(NPTA)** improved film formation ability and miscibility without remarkably depressing aggregation; thus, the donor/acceptor interpenetrating network and desired nanophase separation were achieved.

CONCLUSION

We demonstrate the first attempt to introduce **PTA** and **NPTA** into solution-processed D/A-type small molecules, namely, **DPP_2(PTA)** and **DPP_2(NPTA)**, for OSCs. A systematic study on the optoelectronic and morphology characteristics of two promising small-molecule donors with only the bridgehead atom (sulfur vs nitrogen) of the thienoacene unit as the difference has been performed. The replacement of the bridging atom, thus forming heterocycles with different electronic structures, has a visible effect on both the optical and electrical properties. Owing to the more electron-rich pyrrole, **DPP_2(NPTA)** possesses a broad absorption covering the wavelength range 450−720 nm in solution, which is obviously red-shifted relative to that (450−680 nm) of **DPP_2(PTA)**. Concomitantly, one finds an obvious drop in the HOMO levels for molecules with the bridged atom changing from nitrogen to sulfur.

More importantly, the replacement of the bridging atoms significantly modulates the self-assembly and crystallization behavior and also the formation of crystalline domains in thin film blends with $PC_{71}BM$, which may be due to different substituting alkyl chains on the bridging atoms. **DPP_2(PTA)** shows a high crystallinity but low miscibility with $PC_{71}BM$ due to no alkyl chain substituting on the sulfur atom of the **PTA** unit, while probably, with the aid of a dodecyl chain substituting on the nitrogen atom of the **NPTA** unit, the crystallinity and miscibility with $PC_{71}BM$ for **DPP_2(NPTA)** are largely improved.

Meanwhile, the OSCs based on the two small molecules with $PC_{71}BM$ display a promising performance. The optimized solar cells based on **DPP_2(NPTA)**/$PC_{71}BM$ (1.5:1, w/w) have resulted in PCE up to 3.83% with J_{sc} of 10.69 mA cm^{-2}, V_{oc} of 0.71 V, and FF of 48.3%. This work shows for the first time that **NPTA** is a quite promising donor building block for the construction of high-efficiency D/A-type photoactive materials. Moreover, the work presented in this contribution also provides a guideline for tailoring the relative properties (energy level, crystallinity, especially for morphology) via subtle structural modifications for the design of new organic small-molecule series in pursuit of high-efficiency OSCs.

EXPERIMENTAL SECTION

1. Materials. All reagents were obtained from commercial suppliers and used as received. Tetrahydrofuran (THF) was dried over sodium/benzophenoneketyl and freshly distilled prior to use. Bis[2,2′-(3-bromo-6-hexylthieno[3,2-*b*]thienyl)] (**1**)[68] and 2,5-bis(2-ethylhexyl)-3-(5-bromothiophen-2-yl)-6-(thiophen-2-yl)pyrrolo[3,4-*c*]pyrrole-1,4-(2*H*,5*H*)-dione (**4**)[23] were synthesized according to the reported procedures.

2. Measurements and Instruments. NMR spectra were recorded on a Bruker DPX 400 (^{1}H NMR 400 MHz and ^{13}C NMR 100 MHz) spectrometer. The mass spectra were obtained using an Ion-Spec 4.7 T HiResMALDI instrument. UV absorption spectra were obtained using a Scinco S-3150 UV/vis spectrophotometer. TGA measurements were performed on a Netzsch TG209 apparatus. DSC measurements were performed on a PE DSC 7 calorimeter with about 5 mg samples at a rate of 10 °C min^{-1}. The electrochemical cyclic voltammogram was obtained using a CHI 660C electrochemical workstation with a platinum disk, a platinum plate, and SCE as the working, counter, and reference electrodes, respectively, in a 0.1 mol L^{-1} tetrabutylammonium hexafluorophosphate (Bu_4NPF_6)/CH_2Cl_2 solution. WAXS measurements were carried out using a SAXSess mc2 (Anton Paar) apparatus; the powdered samples were wrapped with aluminum foil for characterization. Topographic images of the films were obtained on a Veeco MultiMode atomic force microscope in the tapping mode.

3. Fabrication and Characterization. Solar cells were fabricated on glass substrates commercially precoated with a layer of indium−tin oxide (ITO). Prior to fabrication, the substrates were cleaned using detergent, deionized water, acetone, and isopropyl alcohol consecutively every 15 min and then treated in an UV-ozone generator for 15 min before being spin-coated with a layer of 35 nm PEDOT:PSS (Baytron P 4083, Germany). After baking PEDOT:PSS in air at 140 °C for 15 min, the substrates were transferred to a glovebox. The BHJ layer was spin-cast at 2500−4000 rpm from a solution of small

dx.doi.org/10.1021/am5006223 | ACS Appl. Mater. Interfaces 2014, 6, 5798−5809

molecules and $PC_{71}BM$ with different blend ratios in chloroform with or without a small content of DIO at a total solid concentration of 20 mg mL^{-1}. The thickness of the photoactive layer is 120 ± 20 nm (calibrated by an Ambios Technology XP-2 profilometer). The interlayer material was dissolved in highly polar solvents such as methanol under the presence of a small amount of acetic acid, and its solution was spin-coated on the top of the obtained active layer to form a thin interlayer of 5 nm. Then the samples were loaded into a vacuum deposition chamber (background pressure ≈ 5×10^{-4} Pa) to deposit 100-nm-thick aluminum cathode with a shadow mask (device area of 5.2 mm^2). *J*–*V* characteristics of the devices in the dark and under illumination were recorded on a Keithley 2400-SCS semiconductor parameter analyzer in air. A Thermal Oriel solar simulator was used to give AM 1.5G irradiance of 100 mW cm^{-2}. EQE spectra were measured using a Stanford 8300 lock-in amplifier unit coupled with a WDG3 monochromator and a 500 W xenon lamp.

The hole mobility of the blends was measured using the SCLC method. Hole-only devices were fabricated in a structure of ITO/PEDOT:PSS/pure small molecules or small molecules/$PC_{71}BM$ blend/MoO_3(10 nm)/Al (100 nm). The device characteristics were extracted by modeling the dark current under forward bias using the SCLC expression described by the Mott–Gurney law.

4. Synthetical Procedures. ***PTA***. Compound **1** (412 mg, 0.68 mmol) was dissolved in dry THF (20 mL). To this mixture was added *n*-BuLi (0.63 mL, 2.5 M in hexane) dropwise at −78 °C under argon. The resulting solution was kept at −78 °C for 15 min before bis(phenylsulfonyl) sulfide (220 mg, 0.7 mmol) was added. The resulting mixture was stirred overnight at room temperature and quenched with water. After most of the THF was evaporated, the mixture was dissolved in hexane (100 mL), washed with water (50 mL), and dried over anhydrous $MgSO_4$. After removal of the solvent under reduced pressure, the residue was purified by column chromatography on silica gel (petroleum ether:CH_2Cl_2 = 5:1), affording a white solid (158 mg, 33%). ^{1}H NMR (400 MHz, $CDCl_3$): δ 6.97 (s, 2H), 2.74 (t, *J* = 7.6 Hz, 4H), 1.97–1.69 (m, 4H), 1.53–1.13 (m, 12H), 0.91 (t, *J* = 6.9 Hz, 6H). ^{13}C NMR (100 MHz, $CDCl_3$): δ 140.74, 136.21, 132.98, 131.62, 131.20, 120.43, 77.34, 77.02, 76.71, 31.62, 29.66, 29.05, 28.68, 22.61, 14.09. MS (ESI). Calcd for $C_{24}H_{28}S_5$: *m*/*z* 476.08. Found: *m*/*z* 477.2 (M^+ + 1).

NPTA. Compound **1** (0.86 g, 1.43 mmol), *t*-BuONa (0.32 g, 3.33 mmol), Pd_2dba_3 (0.031 g, 0.034 mmol), and 1,1′-binaphthalene-2,2′-diylbis(diphenylphosphine) (BINAP; 0.086 g, 0.14 mmol) were dissolved in dry toluene (20 mL). The solution was purged with argon for 10 min, and dodecylamine (0.286 g, 1.54 mmol) was added via a syringe. The mixture was allowed to reflux overnight under an argon atmosphere. Then the reaction was quenched with 20 mL of cold water, and the layers were separated. The aqueous phase was extracted with CH_2Cl_2 three times. The combined organic layers were washed with water and then dried over anhydrous Na_2SO_4. After removal of the solvent under reduced pressure, the residue was purified by column chromatography on silica gel (petroleum ether) to provide the title compound as a yellow solid (0.359 g, 40%). ^{1}H NMR (400 MHz, $CDCl_3$): δ 6.88 (s, 2H), 4.36 (t, *J* = 7.0 Hz, 2H), 2.74 (t, *J* = 7.6 Hz, 4H), 2.08–1.89 (m, 2H), 1.79 (dt, *J* = 15.3 and 7.5 Hz, 4H), 1.51–1.22 (m, 30H), 0.94–0.83 (m, 9H). ^{13}C NMR (100 MHz, $CDCl_3$): δ 138.89, 136.60, 135.03, 123.00, 117.92, 117.07, 48.41, 32.01, 31.74, 31.64, 29.69, 29.63, 29.54, 29.47, 29.43, 29.32, 29.22, 28.79, 26.92, 22.79, 22.71, 14.19. MALDI-TOF-MS. Calcd for $C_{36}H_{53}NS_4$: *m*/*z* 627.30. Found: *m*/*z* 627.3.

Compound **2**: To a solution of **PTA** (0.143 g, 0.23 mmol) in anhydrous THF (20 mL) was added *n*-BuLi (0.23 mL, 2.5 M in hexane) at −78 °C under argon protection. The solution was warmed to room temperature for 30 min and cooled again to −78 °C. Isopropoxyboronic acid/pinacol ester (0.21 g, 1.13 mmol) was injected into the solution in one portion using a syringe. The resulting mixture was stirred at −78 °C for 1 h, left to stir overnight at room temperature, and then quenched with water. After most of the THF was evaporated, the mixture was extracted with CH_2Cl_2, washed with brine and water, and dried over $MgSO_4$. After removal of the solvent under reduced pressure, the residue was purified by column chromatography on silica gel (petroleum ether:CH_2Cl_2 = 5:1), affording a pale yellow oil (70 mg, 35%). ^{1}H NMR (400 MHz, $CDCl_3$): δ 2.72 (t, *J* = 7.6 Hz, 4H), 1.85–1.68 (m, 4H), 1.38–1.27 (m, 36H), 0.92 (t, *J* = 5.6 Hz, 6H). MALDI-TOF-MS. Calcd for $C_{36}H_{50}B_2O_4S_5$: *m*/*z* 728.25. Found: *m*/*z* 728.3.

Compound **3**: **3** was synthesized by the same procedure as that of **2**, affording a pale yellow oil (0.232 g, 40%). ^{1}H NMR (400 MHz, $CDCl_3$): δ 4.35 (t, *J* = 7.0 Hz, 2H), 2.74 (t, *J* = 7.6 Hz, 4H), 2.12–1.89 (m, 2H), 1.79 (dd, *J* = 15.0 and 7.5 Hz, 4H), 1.32–1.21 (m, 54H), 1.00–0.70 (m, 9H). MALDI-TOF-MS. Calcd for $C_{48}H_{75}B_2NO_4S_4$: *m*/*z* 879.47. Found: *m*/*z* 879.5.

DPP$_2$(PTA). A mixture of compound **2** (86 mg, 0.098 mmol), compound **4** (147 mg, 0.24 mmol), aqueous 2 M K_2CO_3 (0.3 mL, 0.6 mmol), Aliquat 336 (2 drops), and toluene (6 mL) was carefully degassed for 20 min before and after the addition of $Pd(PPh_3)_4$ (28 mg, 0.024 mmol). Then the resulting mixture was heated to 85 °C and stirred under a nitrogen atmosphere for 24 h. Water and CH_2Cl_2 were added, the organic layer was separated, the aqueous layer was extracted with CH_2Cl_2, and the combined organic layers were dried over anhydrous $MgSO_4$. After removal of the solvent under reduced pressure, the residue was purified by column chromatography on silica gel (petroleum ether:CH_2Cl_2 = 1:1) to afford **DPP$_2$(PTA)** as a blue-black solid (50 mg, 40%). ^{1}H NMR (400 MHz, $CDCl_3$): δ 9.01 (d, *J* = 4.1 Hz, 2H), 8.88 (s, 2H), 7.51 (d, *J* = 4.5 Hz, 2H), 7.22–7.10 (m, 2H), 3.98 (d, *J* = 8.4 Hz, 8H), 2.80 (t, *J* = 8.0 Hz, 4H), 1.91 (m, 4H), 1.84–1.71 (m, 4H), 1.46–1.25 (m, 44H), 0.90 (m, 30H). ^{13}C NMR (100 MHz, $CDCl_3$): δ 161.46, 161.35, 161.23, 150.40, 143.23, 142.50, 141.72, 140.58, 139.54, 139.43, 139.35, 137.99, 136.60, 135.76, 135.18, 134.36, 133.50, 133.43, 133.28, 132.86, 132.23, 131.62, 131.04, 130.67, 130.12, 130.02, 129.89, 129.79, 129.70, 128.89, 128.63, 128.43, 128.30, 127.92, 125.87, 113.64, 107.99, 107.90, 107.83, 96.28, 77.34, 77.02, 76.70, 73.23, 54.56, 46.13, 46.05, 45.93, 40.17, 39.38, 39.27, 39.14, 34.95, 32.09, 31.81, 31.72, 31.61, 31.33, 30.83, 30.22, 29.93, 29.70, 29.59, 29.43, 29.09, 28.90, 28.70, 28.45, 28.38, 27.59, 26.63, 25.83, 25.35, 24.77, 23.58, 23.53, 23.38, 23.26, 23.19, 23.12, 22.80, 22.69, 15.85, 14.14, 14.11, 14.04, 12.56, 10.53, 10.48, 7.07. MALDI-TOF-MS. Calcd for $C_{84}H_{104}N_4O_4S_9$: *m*/*z* 1520.6. Found: *m*/*z* 1520.3. HRMS (MALDI/DHB): Calcd for $C_{84}H_{104}N_4O_4S_9$: *m*/*z* 1520.5544. Found: *m*/*z* 1520.5536 ± 0.004.

DPP$_2$(NPTA). Compound **DPP$_2$(NPTA)** was synthesized by the same procedure as that of **DPP$_2$(PTA)**, affording a blue-black solid (41 mg, 25%). ^{1}H NMR (400 MHz, $CDCl_3$): δ 9.11 (d, *J* = 4.1 Hz, 2H), 8.88 (s, 2H), 7.50 (d, *J* = 4.5 Hz, 2H), 7.24–7.12 (m, 4H), 4.24 (t, *J* = 4.3 Hz, 2H), 4.12–3.84 (m, 8H), 3.02–2.73 (m, 4H), 2.04 (m, 2H), 2.00–1.83 (m, 4H), 1.83–1.72 (m, 4H), 1.48–1.09 (m, 62H), 1.00–0.70 (m, 33H). ^{13}C NMR (100 MHz, $CDCl_3$): δ 161.59, 161.33, 142.48, 141.87, 141.35, 139.78, 139.04, 136.80, 135.59, 135.21, 134.95, 134.39, 130.00, 129.03, 128.28, 125.04, 121.15, 118.18, 108.10, 107.70, 77.35, 77.23, 77.03, 76.71, 48.56, 46.11, 45.96, 39.36, 39.17, 32.22, 31.87, 31.74, 31.58, 31.44, 30.25, 30.21, 29.70, 29.61, 29.58, 29.57, 29.39, 29.31, 28.95, 28.43, 28.39, 26.89, 26.41, 23.58, 23.42, 23.21, 23.12, 22.67, 22.65, 14.11, 14.07, 14.04, 10.52, 1.02. MALDI-TOF-MS. Calcd for $C_{96}H_{129}N_5O_4S_8$: *m*/*z* 1671.8. Found: *m*/*z* 1671.8. HRMS (MALDI/DHB). Calcd for $C_{96}H_{129}N_5O_4S_8$: *m*/*z* 1671.7810. Found: *m*/*z* 1671.7834 ± 0.005.

■ ASSOCIATED CONTENT

Supporting Information

^{1}H and ^{13}C NMR spectra, DFT-B3LYP/6-31G*-calculated electronic wave functions of HOMO and LUMO based on optimized geometries, and additional *J*–*V* characteristics, and EQE curves of the OSCs based on two small molecules. This material is available free of charge via the Internet at http://pubs.acs.org.

■ AUTHOR INFORMATION

Corresponding Authors

*E-mail: wan_junhua@hznu.edu.cn.

*E-mail: minminshi@zju.edu.cn.

Author Contributions

‡These authors contributed equally.

Notes

The authors declare no competing financial interest.

■ ACKNOWLEDGMENTS

This work was supported by the National Natural Science Foundation of China (No. 21372057). The authors also thank Dr. Feng Liu (University of Massachusetts) for his help discussion.

■ REFERENCES

(1) Roncali, J. Molecular Bulk Heterojunctions: an Emerging Approach to Organic Solar Cells. *Acc. Chem. Res.* **2009**, *42*, 1719−1730.

(2) Walker, B.; Kim, C.; Nguyen, T.-Q. Small Molecule Solution-Processed Bulk Heterojunction Solar Cells. *Chem. Mater.* **2011**, *23*, 470−482.

(3) Chen, Y. S.; Wan, X. J.; Long, G. High Performance Photovoltaic Applications Using Solution-Processed Small Molecules. *Acc. Chem. Res.* **2013**, *46*, 2645−2655.

(4) Lin, Y.; Li, Y. F.; Zhan, X. W. Small Molecule Semiconductors for High-Efficiency Organic Photovoltaics. *Chem. Soc. Rev.* **2012**, *41*, 4245−4272.

(5) Li, Y.; Guo, Q.; Li, Z.; Pei, J.; Tian, W.J Solution Processable D−A Small Molecules for Bulk-Heterojunction Solar Cells. *Energy Environ. Sci.* **2010**, *3*, 1427−1436.

(6) Mishra, A.; Bauerle, P. Small Molecule Organic Semiconductors on the Move: Promises for Future Solar Energy Technology. *Angew. Chem., Int. Ed.* **2012**, *51*, 2020−2067.

(7) Zhou, J.; Zuo, Y.; Wan, X. J.; Long, G.; Zhang, Q.; Ni, W.; Liu, Y.; Li, Z.; He, G.; Li, C.; Kan, B.; Li, M.; Chen, Y. S. Solution-Processed and High-Performance Organic Solar Cells Using Small Molecules with a Benzodithiophene Unit. *J. Am. Chem. Soc.* **2013**, *135*, 8484−8487.

(8) Kyaw, A. K.; Wang, D. H.; Gupta, V.; Zhang, J.; Chand, S.; Bazan, G. C.; Heeger, A. J. Efficient Solution-Processed Small-Molecule Solar Cells with Inverted Structure. *Adv. Mater.* **2013**, *25*, 2397−2402.

(9) Zhou, J.; Wan, X. J.; Liu, Y.; Zuo, Y.; Li, Z.; He, G.; Long, G.; Ni, W.; Li, C.; Su, X.; Chen, Y. S. Small Molecules Based on Benzo[1,2-*b*:4,5-*b*′]dithiophene Unit for High-Performance Solution-Processed Organic Solar Cells. *J. Am. Chem. Soc.* **2012**, *134*, 16345−16351.

(10) Liu, Y.; Chen, C. C.; Hong, Z.; Gao, J.; Michael Yang, Y.; Zhou, H.; Dou, L.; Li, G.; Yang, Y. Solution-Processed Small-Molecule Solar Cells: Breaking the 10% Power Conversion Efficiency. *Sci. Rep.* **2013**, *3*, 3356.

(11) Kyaw, A. K. K.; Wang, D. H.; Gupta, V.; Leong, W. L.; Ke, L.; Bazan, G. C.; Heeger, A. J. Intensity Dependence of Current−Voltage Characteristics and Recombination in High-Efficiency Solution-Processed Small-Molecule Solar Cells. *ACS Nano* **2013**, *7*, 4569−4577.

(12) Li, W. W.; Kelchtermances, M.; Wienki, M. M.; Janssen, R. A. J. Effect of Structure on The Solubility and Photovoltaic Properties of Bis-Diketopyrrolopyrrole Molecules. *J. Mater. Chem. A* **2013**, *1*, 15150−15157.

(13) Yang, X.; Veenstra, S. C.; Verhees, W.; Wienk, J. H.; Janssen, M. M.; Kroon, R. A. J.; Michels, J. M.; Loos, M. A. J.; Nanoscale, J. Morphology of High-Performance Polymer Solar Cells. *Nano Lett.* **2005**, *5*, 579−583.

(14) Zhou, H.; Yang, L.; You, W. Rational Design of High Performance Conjugated Polymers for Organic Solar Cells. *Macromolecules* **2012**, *45*, 607−632.

(15) McCulloch, I.; Ashraf, R. S.; Biniek, L.; Bronstein, H.; Combe, C.; Donaghey, J. E.; James, D. I.; Nielsen, C. B.; Schroeder, B. C.; Zhang, W. Design of Semiconducting Indacenodithiophene Polymers for High Performance Transistors and Solar Cells. *Acc. Chem. Res.* **2012**, *45*, 714−722.

(16) Facchetti, A. π-Conjugated Polymers for Organic Electronics and Photovoltaic Cell Applications. *Chem. Mater.* **2011**, *23*, 733−758.

(17) Zhou, J.; Wan, X. J.; Liu, Y.; Long, G.; Wang, F.; Li, Z.; Zuo, Y.; Li, C.; Chen, Y. S. A Planar Small Molecule with Dithienosilole Core for High Efficiency Solution-Processed Organic Photovoltaic Cells. *Chem. Mater.* **2011**, *23*, 4666−4668.

(18) Sun, Y.; Welch, G. C.; Leong, W. L.; Takacs, C. J.; Bazan, G. C.; Heeger, A. J. Solution-Processed Small-Molecule Solar Cells with 6.7% Efficiency. *Nat. Mater.* **2011**, *11*, 44−48.

(19) Dutta, P.; Yang, W.; Eom, S. H.; Lee, W. H.; Kang, I. N.; Lee, S. H. Development of Naphtho[1,2-*b*:5,6-*b*′]dithiophene Based Novel Small Molecules for Efficient Bulk-Heterojunction Organic Solar Cells. *Chem. Commun. (Camb.)* **2012**, *48*, 573−575.

(20) Patra, D.; Huang, T. Y.; Chiang, C. C.; Maturana, R. O.; Pao, C. W.; Ho, K. C.; Wei, K. H.; Chu, C. W. 2-Alkyl-5-thienyl-substituted Benzo[1,2-*b*:4,5-*b*′]dithiophene-Based Donor Molecules for Solution-Processed Organic Solar Cells. *ACS Appl. Mater. Interfaces* **2013**, *5*, 9494−9500.

(21) He, M.; Li, J.; Sorensen, M. L.; Zhang, F.; Hancock, R. R.; Fong, H. H.; Pozdin, V. A.; Smilgies, D.-M.; Malliaras, G. G. Alkylsubstituted Thienothiophene Semiconducting Materials: Structure−Property Relationships. *J. Am. Chem. Soc.* **2009**, *131*, 11930−11938.

(22) Peng, Q.; Huang, Q.; Hou, X.; Chang, P.; Xu, J.; Deng, S. Enhanced Solar Cell Performance by Replacing Benzodithiophene with Naphthodithiophene in Diketopyrrolopyrrole-Based Copolymers. *Chem. Commun. (Camb.)* **2012**, *48*, 11452−11454.

(23) Loser, S.; Bruns, C. J.; Miyauchi, H.; Ortiz, R. P.; Facchetti, A.; Stupp, S. I.; Marks, T. J. A Naphthodithiophene−Diketopyrrolopyrrole Donor Molecule for Efficient Solution-Processed Solar Cells. *J. Am. Chem. Soc.* **2011**, *133*, 8142−8145.

(24) Loser, S.; Miyauchi, H.; Hennek, J. W.; Smith, J.; Huang, C.; Facchetti, A.; Marks, T. J. A "Zig-Zag" Naphthodithiophene Core for Increased Efficiency in Solution-Processed Small Molecule Solar Cells. *Chem. Commun. (Camb.)* **2012**, *48*, 8511−8513.

(25) Guerrero, A.; Loser, S.; Garcia-Belmonte, G.; Bruns, C. J.; Smith, J.; Miyauchi, H.; Stupp, S. I.; Bisquert, J.; Marks, T. J. Solution-Processed Small Molecule: Fullerene Bulk-Heterojunction Solar Cells: Impedance Spectroscopy Deduced Bulk and Interfacial Limits to Fill-Factors. *Phys. Chem. Chem. Phys.* **2013**, *15*, 16456−62.

(26) Moulé, A. J.; Tsami, A.; Bünnagel, T. W.; Forster, M.; Kronenberg, N. M.; Scharber, M.; Koppe, M.; Morana, M.; Brabec, C. J.; Meerholz, K. Two Novel Cyclopentadithiophene-Based Alternating Copolymers as Potential Donor Components for High-Efficiency Bulk-Heterojunction-Type Solar Cells. *Chem. Mater.* **2008**, *20*, 4045−4050.

(27) Horie, M.; Kettle, J.; Yu, C.-Y.; Majewski, L. A.; Chang, S.-W.; Kirkpatrick, J.; Tuladhar, S. M.; Nelson, J.; Saunders, B. R.; Turner, M. L. Cyclopentadithiophene−Benzothiadiazole Oligomers and Polymers; Synthesis, Characterisation, Field-Effect Transistor and Photovoltaic Characteristics. *J. Mater. Chem.* **2012**, *22*, 381.

(28) Li, Y.; Zou, J.; Yip, H.-L.; Li, C.-Z.; Zhang, Y.; Chueh, C.-C.; Intemann, J.; Xu, Y.; Liang, P.-W.; Chen, Y.; Jen, A. K. Y. Side-Chain Effect on Cyclopentadithiophene/Fluorobenzothiadiazole-Based Low Band Gap Polymers and Their Applications for Polymer Solar Cells. *Macromolecules* **2013**, *46*, 5497−5503.

(29) Hou, J. H.; Chen, H.-Y.; Zhang, S.; Li, G.; Yang, Y. Synthesis, Characterization, and Photovoltaic Properties of a Low Band Gap Polymer Based on Silole-Containing Polythiophenes and 2,1,3-Benzothiadiazole. *J. Am. Chem. Soc.* **2008**, *130*, 16144−16145.

(30) Beaujuge, P. M.; Pisula, W.; Tsao, H. N.; Ellinger, S.; Müllen, K.; Reynolds, J. R. Tailoring Structure− Property Relationships in Dithienosilole−Benzothiadiazole Donor−Acceptor Copolymers. *J. Am. Chem. Soc.* **2009**, *131*, 7514−7515..

(31) Chu, T. Y.; Lu, J.; Beaupre, S.; Zhang, Y.; Pouliot, J. R.; Wakim, S.; Zhou, J.; Leclerc, M.; Li, Z.; Ding, J.; Tao, Y. Bulk Heterojunction Solar Cells Using Thieno[3,4-*c*]pyrrole-4,6-dione and Dithieno[3,2-*b*:2′,3′-*d*]silole Copolymer with a Power Conversion Efficiency of 7.3%. *J. Am. Chem. Soc.* **2011**, *133*, 4250−4253.

(32) Liu, J.; Zhang, R.; Osaka, I.; Mishra, S.; Javier, A. E.; Smilgies, D.-M.; Kowalewski, T.; McCullough, R. D. Transistor Paint: Environmentally Stable *N*-Alkyldithienopyrrole and Bithiazole-Based Copolymer Thin-Film Transistors Show Reproducible High Mobilities without Annealing. *Adv. Funct. Mater.* **2009**, *19*, 3427−3434.
(33) Zhou, E.; Cong, J.; Tajima, K.; Hashimoto, K. Synthesis and Photovoltaic Properties of Donor−Acceptor Copolymers Based on 5,8-Dithien-2-yl-2,3-diphenylquinoxaline. *Chem. Mater.* **2010**, *22*, 4890−4895.
(34) Wunsch, B. H.; Rumi, M.; Tummala, N. R.; Risko, C.; Kang, D.-Y.; Steirer, K. X.; Gantz, J.; Said, M.; Armstrong, N. R.; Brédas, J.-L.; Bucknall, D.; Marder, S. R. Structure−Processing−Property Correlations in Solution-Processed, Small-Molecule, Organic Solar Cells. *J. Mater. Chem. C* **2013**, *1*, 5250−5260.
(35) Weidelener, M.; Wessendorf, C. D.; Hanisch, J.; Ahlswede, E.; Gotz, G.; Linden, M.; Schulz, G.; Mena-Osteritz, E.; Mishra, A.; Bauerle, P. Dithienopyrrole-Based Oligothiophenes for Solution-Processed Organic Solar Cells. *Chem. Commun. (Camb.)* **2013**, *49*, 10865−10867.
(36) Park, J. K.; Kim, C.; Walker, B.; Nguyen, T.-Q.; Seo, J. H. Morphology Control of Solution Processable Small Molecule Bulk Heterojunction Solar Cells via Solvent Additives. *RSC Adv.* **2012**, *2*, 2232.
(37) Li, J.; Tan, H.-S.; Chen, Z.-K.; Goh, W.-P.; Wong, H.-K.; Ong, K.-H.; Liu, W.; Li, C. M.; Ong, B. S. Dialkyl-Substituted Dithienothiophene Copolymers as Polymer Semiconductors for Thin-Film Transistors and Bulk Heterojunction Solar Cells. *Macromolecules* **2011**, *44*, 690−693.
(38) Huang, X. B.; Zhu, C. L.; Zhang, S. M.; Li, W. W.; Guo, Y. L.; Zhan, X. W.; Liu, Y. Q.; Bo, Z. S. Porphyrin−Dithienothiophene π-Conjugated Copolymers: Synthesis and Their Applications in Field-Effect Transistors and Solar Cells. *Macromolecules* **2008**, *41*, 6895−6902.
(39) Patil, A. V.; Lee, W.-H.; Lee, E.; Kim, K.; Kang, I.-N.; Lee, S.-H. Synthesis and Photovoltaic Properties of a Low-Band-Gap Copolymer of Dithieno[3,2-*b*:2′,3′-*d*]thiophene and Dithienylquinoxaline. *Macromolecules* **2011**, *44*, 1238−1241.
(40) Polander, L. E.; Tiwari, S. P.; Pandey, L.; Seifried, B. M.; Zhang, Q.; Barlow, S.; Risko, C.; Brédas, J.-L.; Kippelen, B.; Marder, S. R. Solution-Processed Molecular Bis(naphthalene diimide) Derivatives with High Electron Mobility. *Chem. Mater.* **2011**, *23*, 3408−3410.
(41) Shinamura, S.; Osaka, I.; Miyazaki, E.; Nakao, A.; Yamagishi, M.; Takeya, J.; Takimiya, K. Linear- and Angular-Shaped Naphthodithiophenes: Selective Synthesis, Properties, and Application to Organic Field-Effect Transistors. *J. Am. Chem. Soc.* **2011**, *133*, 5024−5035.
(42) Chen, Y.-L.; Chang, C.-Y.; Cheng, Y.-J.; Hsu, C.-S. Synthesis of a New Ladder-Type Benzodi(cyclopentadithiophene) Arene with Forced Planarization Leading to an Enhanced Efficiency of Organic Photovoltaics. *Chem. Mater.* **2012**, *24*, 3964−3971.
(43) Kim, J.; Han, A. R.; Seo, J. H.; Oh, J. H.; Yang, C. β-Alkyl substituted Dithieno[2,3-*d*;2′,3′-*d*′]benzo[1,2-*b*;4,5-*b*′]dithiophene Semiconducting Materials and Their Application to Solution-Processed Organic Transistors. *Chem. Mater.* **2012**, *24*, 3464−3472.
(44) Zeng, Z.; Li, Y.; Deng, J. F.; Huang, Q.; Peng, Q. Synthesis and Photovoltaic Performance of Low Band Bap Copolymers Based on Diketopyrrolopyrrole and Tetrathienoacene with Different Conjugated Bridges. *J. Mater. Chem. A* **2014**, *2*, 653−662.
(45) Xiao, K.; Liu, Y.; Qi, T.; Zhang, W.; Wang, F.; Gao, J.; Qiu, W.; Ma, Y.; Cui, G.; Chen, S. A Highly π-Stacked Organic Semiconductor for Field-Effect Transistors Based on Linearly Condensed Pentathienoacene. *J. Am. Chem. Soc.* **2005**, *127*, 13281−13286.
(46) Qu, S.; Tian, H. Diketopyrrolopyrrole (DPP)-Based Materials for Organic Photovoltaics. *Chem. Commun. (Camb.)* **2012**, *48*, 3039−3051.
(47) Lee, O. P.; Yiu, A. T.; Beaujuge, P. M.; Woo, C. H.; Holcombe, T. W.; Millstone, J. E.; Douglas, J. D.; Chen, M. S.; Frechet, J. M. Efficient Small Molecule Bulk Heterojunction Solar Cells with High Fill Factors via Pyrene-Directed Molecular Self-Assembly. *Adv. Mater.* **2011**, *23*, 5359−5363.
(48) Huang, J.; Zhan, C.; Zhang, X.; Zhao, Y.; Lu, Z.; Jia, H.; Jiang, B.; Ye, J.; Zhang, S.; Tang, A.; Liu, Y.; Pei, Q.; Yao, J. Solution-processed DPP-Based Small Molecule That Gives High Photovoltaic Efficiency with Judicious Device Optimization. *ACS Appl. Mater. Interfaces* **2013**, *5*, 2033−2039.
(49) Shin, W.; Yasuda, T.; Watanabe, G.; Yang, Y. S.; Adachi, C. Self-Organizing Mesomorphic Diketopyrrolopyrrole Derivatives for Efficient Solution-Processed Organic Solar Cells. *Chem. Mater.* **2013**, *25*, 2549−2556.
(50) Mei, J. G.; Graham, K. R.; Stalder, R.; Tiwari, S. P.; Cheun, H.; Shim, J.; Yoshio, M.; Nuckolls, C.; Kippelen, B.; Castellano, R. K.; Reynolds, J. R. Self-Assembled Amphiphilic Diketopyrrolopyrrole-Based Oligothiophenes for Field-Effect Transistors and Solar Cells. *Chem. Mater.* **2011**, *23*, 2285−2288.
(51) Qian, G.; Qi, J.; Davey, J. A.; Wright, J. S.; Wang, Z. Y. Family of Diazapentalene Chromophores and Narrow-Band-Gap Polymers: Synthesis, Halochromism, Halofluorism, and Visible−Near-Infrared Photodetectivity. *Chem. Mater.* **2012**, *24*, 2364−2372.
(52) Bura, T.; Leclerc, N.; Bechara, R.; Lévêque, P.; Heiser, T.; Ziessel, R. Solar Cells: Triazatruxene−Diketopyrrolopyrrole Dumbbell-Shaped Molecules as Photoactive Electron Donor for High-Efficiency Solution Processed Organic Solar Cells. *Adv. Energy Mater.* **2013**, *3*, 1109−1109.
(53) Eisenmenger, N. D.; Su, G. M.; Welch, G. C.; Takacs, C. J.; Bazan, G. C.; Kramer, E. J.; Chabinyc, M. L. Effect of Bridging Atom Identity on the Morphological Behavior of Solution-Processed Small Molecule Bulk Heterojunction Photovoltaics. *Chem. Mater.* **2013**, *25*, 1688−1698.
(54) Mei, J. G.; Diao, Y.; Appleton, A. L.; Fang, L.; Bao, Z. Integrated Materials Design of Organic Semiconductors for Field-Effect Transistors. *J. Am. Chem. Soc.* **2013**, *135*, 6724−6746.
(55) Gevaerts, V. S.; Herzig, E. M.; Kirkus, M.; Hendriks, K. H.; Wienk, M. M.; Perlich, J.; Müller-Buschbaum, P.; Janssen, R. A. J. Influence of the Position of the Side Chain on Crystallization and Solar Cell Performance of DPP-Based Small Molecules. *Chem. Mater.* **2014**, *26*, 916−926.
(56) Liu, X.; Sun, Y.; Perez, L. A.; Wen, W.; Toney, M. F.; Heeger, A. J.; Bazan, G. C. Narrow-Band-Gap Conjugated Chromophores with Extended Molecular Lengths. *J. Am. Chem. Soc.* **2012**, *134*, 20609−20612.
(57) Takacs, C. J.; Sun, Y.; Welch, G. C.; Perez, L. A.; Liu, X.; Wen, W.; Bazan, G. C.; Heeger, A. J. Solar Cell Efficiency, Self-Assembly, and Dipole−Dipole Interactions of Isomorphic Narrow-Band-Gap Molecules. *J. Am. Chem. Soc.* **2012**, *134*, 16597−16606.
(58) Wan, J.-H.; Mao, L.-Y.; Li, Y.-B.; Li, Z.-F.; Qiu, H.-Y.; Wang, C.; Lai, G.-Q. Self-assembly of Novel Fluorescent Silole Derivatives into Different Supramolecular Aggregates: Fibre, Liquid Crystal and Monolayer. *Soft Matter* **2010**, *6*, 3195−3201.
(59) Ding, L.; Li, H.-B.; Lei, T.; Ying, H.-Z.; Wang, R.-B.; Zhou, Y.; Su, Z.-M.; Pei, J. Alkylene-Chain Effect on Microwire Growth and Crystal Packing of π-Moieties. *Chem. Mater.* **2012**, *24*, 1944−1949.
(60) Uhrich, C.; Schueppel, R.; Petrich, A.; Pfeiffer, M.; Leo, K.; Brier, E.; Kilickiran, P.; Baeuerle, P. Organic Thin-Film Photovoltaic Cells Based on Oligothiophenes with Reduced Bandgap. *Adv. Funct. Mater.* **2007**, *17*, 2991−2999.
(61) Turbiez, M.; Frere, P.; Allain, M.; Videlot, C.; Ackermann, J.; Roncali, J. Design of Organic Semiconductors: Tuning the Electronic Properties of pConjugated Oligothiophenes with the 3,4-Ethylenedioxythiophene (EDOT) Building Block. *Chem.—Eur. J.* **2005**, *11*, 3742−3752.
(62) Tamayo, A. B.; Walker, B.; Nguyen, T.-Q. A Low Band Gap, Solution Processable Oligothiophene with a Diketopyrrolopyrrole Core for Use in Organic Solar Cells. *J. Phys. Chem. C* **2008**, *112*, 11545−11551.
(63) Shi, Q.; Cheng, P.; Li, Y. F.; Zhan, X. W. A Solution Processable D−A−D Molecule based on Thiazolothiazole for High Performance Organic Solar Cells. *Adv. Energy Mater.* **2012**, *2*, 63−67.
(64) Shen, S.; Jiang, P.; He, C.; Zhang, J.; Shen, P.; Zhang, Y.; Yi, Y.; Zhang, Z.; Li, Z.; Li, Y. F. Solution-Processable Organic Molecule

Photovoltaic Materials with Bithienyl-Benzodithiophene Central Unit and Indenedione End Groups. *Chem. Mater.* **2013**, *25*, 2274−2281.
(65) Wang, H. Y.; Liu, F.; Bu, L.; Gao, J.; Wang, C.; Wei, W.; Russell, T. P. The Role of Additive in Diketopyrrolopyrrole-Based Small Molecular Bulk Heterojunction Solar Cells. *Adv. Mater.* **2013**, *25*, 6519−6525.
(66) Graham, K. R.; Mei, J. G.; Stalder, R.; Shim, J. W.; Cheun, H.; Steffy, F.; So, F.; Kippelen, B.; Reynolds, J. R. Polydimethylsiloxane As a Macromolecular Additive for Enhanced Performance of Molecular Bulk Heterojunction Organic Solar Cells. *ACS Appl. Mater. Interfaces* **2011**, *3*, 1210−1215.
(67) Kippelen, B.; Brédas, J.-L. Organic Photovoltaics. *Energy Environ. Sci.* **2009**, *2*, 251.
(68) Wan, J. H.; Fang, W. F.; Li, Z. F.; Xiao, X. Q.; Xu, Z.; Deng, Y.; Zhang, L. H.; Jiang, J. X.; Qiu, H. Y.; Wu, L. B.; Lai, G. Q. Novel Ladder π-conjugated Materials−Sila-pentathienoacenes: Synthesis, Structure, and Electronic Properties. *Chem.—Asian J.* **2010**, *5*, 2290−2296.